STEM CELLS AND DEVELOPMENT
Volume 22, Number 23, 2013
© Mary Ann Liebert, Inc.
DOI: 10.1089/scd.2013.0119

Grafts Enriched with Subamnion-Cord-Lining Mesenchymal Stem Cell Angiogenic Spheroids Induce Post-Ischemic Myocardial Revascularization and Preserve Cardiac Function in Failing Rat Hearts

Eliana C. Martinez,[1,2] Duc-Thang Vu,[1] Jing Wang,[1] Shera Lilyanna,[1] Lieng H. Ling,[3] Shu U. Gan,[1] Ai Li Tan,[1] Thang T. Phan,[1,4] Chuen N. Lee,[1,5,*] and Theo Kofidis[1,5,*]

A crucial question in post-ischemic cell therapy refers to the ideal method of cell delivery to the heart. We hypothesized that epicardial implantation of subamnion-cord-lining mesenchymal stem cells (CL-MSC) angiogenic spheroids embedded within fibrin grafts (SASG) facilitates donor cell survival and enhances cardiac function in failing rat hearts. Furthermore, we compared the efficacy of this approach applied through two delivery methods. Spheroids made of 1.5×10^4 human CL-MSC coated with 2×10^3 human umbilical vein endothelial cells were self-assembled in hanging drops. SASG were constructed by embedding 150 spheroids in fibrin matrix. Except for untreated rats (MI, $n=8$), grafts were implanted 2 weeks after myocardial infarction upon confirmation of ensued heart failure through thoracotomy: SASG ($n=8$) and fibrin graft (FG, $n=8$); or video-assisted thoracoscopic surgery (VATS): SASG-VATS ($n=8$) and FG-VATS ($n=7$). In vivo CL-MSC survival was comparable between both SASG-treated groups throughout the study. SASG and SASG-VATS animals had decreased left ventricular end-diastolic pressure relative to untreated animals, and increased fractional shortening compared to MI and FG controls, 4 weeks after treatment. A 14.1% and 6.2% enhancement in ejection fraction from week 2 to 6 after injury was observed in SASG/SASG-VATS, paralleled by improvement in cardiac output. Treated hearts had smaller scar size, and more blood vessels than MI, while donor CL-MSC contributed to arteriogenesis within the graft and infarct areas. Taken together, our data suggest that SASG treatment has the potential to restore failing hearts by preserving cardiac function and inducing myocardial revascularization, while attenuating cardiac fibrosis. Furthermore, we introduce a method for minimally invasive in situ graft assembly.

Introduction

One of the most important questions in post-ischemic cell therapy refers to the ideal method of cell delivery to the heart [1]. To date, the application of stem cell therapy into clinical practice for post-ischemic myocardial repair remains modest due to limitations, such as poor stem cell retention, and postengraftment survival after cell delivery through systemic or local injections [1,2]. Scaffold-free cell aggregates constitute an alternative to cell-based therapies for tissue repair [3,4]. Cells arranged in spheroids possess better three-dimensional (3D) cell–cell and cell–matrix interactions and can display more in vivo properties compared to two-dimensional monolayer cell cultures [5]. It has been reported that monolayer culture of bone marrow mesenchymal stem cells (BM-MSC) induces loss of cell-specific properties [6], while BM-MSC spheroids generated in a dynamic cell culture undergo changes in cellular architecture and extracellular matrix (ECM) gene expression, and display enhanced differentiation potential compared to monolayer cultures [7]. ECM provides an optimal niche in vitro in which stem cells efficiently retain their properties [8]; thus, the importance of

[1]Department of Surgery, Yong Loo Lin School of Medicine, National University of Singapore, Singapore, Singapore.
[2]Cardiovascular Research Institute, National University Heart Centre Singapore, Singapore, Singapore.
[3]Department of Medicine, Yong Loo Lin School of Medicine, National University of Singapore, Singapore, Singapore.
[4]CellResearch Corporation Pte, Ltd., Singapore, Singapore.
[5]Department of Cardiac, Thoracic and Vascular Surgery, National University Hospital, Singapore, Singapore.
*These authors contributed equally to this work.

tissue-specific 3D matrix. Self-assembly of cells in hanging drops enables the generation of spheroids with homogeneous size devoid the usage of biomaterials. The hanging drop method has been used to generate multicellular spheroids from a wide variety of primary cells and tumor cell lines [5,9,10], and has been an integral part of cancer research. Self-assembled spheroids produce angiogenic factors which enable prevascularization and promote angiogenesis upon implantation [11]. Also, coating of tissue spheroids with human umbilical vein endothelial cells (HUVEC) produce vascularized microtissues after endothelial cell migration towards the spheroid's core [10].

In a recent study, we assessed the potential of a promising cell type from the umbilical cord subamnion membrane [12,13], namely cord-lining mesenchymal stem cells (CL-MSC) to repair failing hearts. Treatment with monodispersed CL-MSC embedded in a fibrin graft (FG) prevented further deterioration of cardiac function in a model of chronic heart failure in nude rats. However, when the CL-MSC grafts were supplemented with direct vascular supply through an omental flap, it improved myocardial revascularization, and ameliorated cardiac dysfunction through a synergistic effect [14]. In the present study, CL-MSC were used to generate angiogenic spheroids that were allowed to self-assemble in hanging drop cocultures with HUVEC. We assessed the hypothesis that epicardial delivery of subamnion-CL-MSC angiogenic spheroids-enriched grafts (SASG) enables donor cell retention and survival, and enhances cardiac function in failing rat hearts. This hybrid approach combines scaffold-free generated tissue embedded within a fibrin scaffold aiming at providing controlled cell delivery onto the target area in a therapeutically relevant time-point. Furthermore, we compared the efficacy of this approach applied through two different delivery methods, that is, epicardial graft implantation through lateral thoracotomy versus in situ assembly of the epicardial grafts via minimally invasive video-assisted thoracoscopic surgery (VATS). To our knowledge, this is the first study to utilize VATS for in situ cardiac tissue engineering in rats.

Materials and Methods

Assembly of CL-MSC angiogenic spheroids

To produce angiogenic spheroids, 1.5×10^4 human CL-MSC-*GFP-Fluc* were allowed to self-assemble for 3 days in 25 μL serum-free medium hanging drops placed in six-well dishes' lids, and incubated at 37°C in 5% humidified CO_2. The plate's wells were filled with DPBS to avoid drop evaporation. Medium was exchanged every other day. CL-MSC spheroids were then coated at day 4 with 2×10^3 HUVEC in 10 μL medium [10]. Angiogenic spheroids were harvested 3 days after coating (at day 7 in drop culture) and washed with sterile DPBS.

Construction of SASG

Sterile fibrin matrix (Tisseel; Baxter Healthcare Corporation) was prepared after the vendor instructions and used as scaffold material to construct SASG. For in vitro studies, 75 angiogenic spheroids (i.e., CL-MSC spheroids coated with HUVEC) in serum free media were mixed with fibrin matrix (1:4) to a final volume of 125 μL, and plated into eight-well chamber slides (Lab-Tek™II Chamber Slide™; NUNC A/S). This procedure was repeated upon fibrin polymerization for a final volume of 250 μL to produce $10\times8\times2.5$ mm grafts containing 150 spheroids distributed across the graft. Thus, 2.25×10^6 CL-MSC and 3×10^5 HUVEC were contained in each graft. Acellular FGs were used as negative controls. Once polymerized, grafts were covered with 0.4 mL serum free media and placed in an incubator under CO_2 at 37°C. The medium was exchanged daily.

Rat model of myocardial infarction

All experiments were approved by the Institutional Animal Care and Use Committee (IACUC) of the National University of Singapore and carried out in accordance with established guiding principles for animal research. Male NIH nude rats (250–300 g; Taconic) were used. Anaesthesia was induced and maintained with inhalational isoflurane (2%) and intraperitoneal injection of ketamine:xylazine (90:10 mg/kg). Left-thoracotomy and pericardectomy followed by left anterior descending coronary artery (LAD) ligation was performed as previously described [15]. Carprofen (5 mg/kg, SC) and Ceftazoline (15 mg/kg, bid, SC) were administered postoperatively for 1 week. Animals were randomly assigned a therapeutic procedure 2 weeks after myocardial infarction and upon confirmation of fractional area change $\leq 40\%$ by echocardiography.

SASG implantation via lateral thoracotomy

To construct grafts for in vivo studies, spheroids were mixed with DPBS and fibrin matrix to create SASG or FG with same dilution and final volume as per in vitro studies. Grafts were prepared on the same day of implantation. After a second lateral thoracotomy as described above, SASG or FG was implanted onto the scar area using 50 μL of fibrin as attachment material to the epicardium. After the therapeutic procedure, the chest was closed in three layers, and animals were allowed to recover in a small-animal intensive care unit. Carprofen (5 mg/kg, SC) and Ceftazoline (15 mg/kg, bid, SC) were administered postoperatively for 7 days.

SASG implantation via video-assisted thoracoscopic surgery

After general anesthesia and intubation, two 3 mm incisions were made in the rat's left hemithorax to insert the endoscopic instruments. First, a 6-0 silk suture was placed at the fourth to fifth intercostal space to lift the chest wall, followed by a 3-mm incision made at the fourth intercostal space, parasternal line. The second incision was made at the eighth space, mid-axillar line. Next, a 2-mm straight forward telescope (Hopkins II, 0°; Karl Storz Endoscopy) connected to a parfocal zoom camera head (TELECAM) and an integrated digital processing module (Tele Pack; all from Karl Storz) was inserted through the lower incision and advanced through the pleural space until the heart was visualized. Scar tissue between the chest wall and the left ventricular (LV) infarct area was carefully removed using a 2-mm grasping forceps (CLICKin Reddick Olsen; Karl Storz) inserted through the upper incision under video-thoracoscopic visualization.

For in situ construction of SASG via VATS, angiogenic spheroids suspended in DPBS were mixed with fibrin at the

same dilution used for premade grafts (1:4) and delivered onto the area of ischemia in three batches of 50 spheroids in 75 μL of matrix. The mixture was loaded into a 16G catheter (Introcan Safety®, IV Catheter 16G×2 inches; BBraun AG) using a 1-mL syringe and was only advanced to the edge of the catheter to avoid accelerated fibrin polymerization or spheroid entrapment within the syringe. To assemble the epicardial patch in situ, each batch of fibrin-DPBS with (SASG-VATS) or without spheroids (FG-VATS) was allowed to start polymerizing within the 16G catheter for ~45 s. The catheter was then inserted into the thorax using the VATS' upper incision, and the partially gelled mixture was deposited epicardially onto the scar area under video-thoracoscopic visualization. The mixture was allowed to polymerize completely before the next batch was applied. The latter was repeated three times until the scar area was totally covered with spheroids. Finally, a 100-μL layer of DPBS/Fibrin was applied on top of the spheroids layer forming an in situ-created 3D graft ~2.5 mm thick. After the therapeutic procedure, postoperative care was provided as described above.

Additional Materials and Methods section can be found in Supplementary Data (Supplementary Data are available online at www.liebertpub.com/scd).

Statistical analysis

Data are presented as mean ± SD. To test for statistically significant differences between-group comparisons of echocardiographic indexes were performed using a two-way ANOVA with repeated measures followed by pairwise comparisons by Bonferroni's post-test. The ANOVA model included control versus treatment and baseline versus 2 and 6 weeks after MI as factors, as well as the interaction between the two factors. For other comparisons, one-way ANOVA followed by Bonferroni's post hoc test, and unpaired Student's *t*-test were used when appropriate. Differences were considered significant when $P < 0.05$. All statistical analyses were performed using GraphPad Prism® software version 5.04 for Windows (GraphPad Software).

Results

Phenotypic and functional characteristics of CL-MSC

CL-MSC are plastic-adherent cells that have spindle-like, fibroblastic morphology when maintained in standard culture conditions. Multilineage differentiation potential of CL-MSC was confirmed, as cells were differentiable towards chondrogenic, adipogenic and osteogenic lineages (Supplementary Fig. S1A). Lentiviral transduction efficiency studies revealed that 75% of cells were green fluorescent protein (GFP) positive.

Flow cytometry studies indicated that CL-MSC-*GFP-Fluc* expressed the MSC markers CD73 (99%), CD90 (99%), and CD105 (98%) (Supplementary Fig. S1B) [16], and were also positive to CD44 (38%) and CD29 (42.2%). Furthermore, CL-MSC-GFP-Fluc were negative for the endothelial cell marker CD31 (0.1%), and hematopoietic stem cell markers CD34 (0.3%), CD45 (0.3%), and C-kit/CD117 (0.2%). Likewise, CL-MSC-GFP-Fluc did not express the embryonic stem cell marker CD15/SSEA-1 (1.1%) [17,18]. As previously described,[16] CL-MSC-*GFP-Fluc* were insignificantly positive to CD14 (6.8%) (Supplementary Fig. S1C).

CL-MSC spheroids coated with HUVECs display enhanced expression of VEGF dimers

By using gravity-enforced self-assembly, we produced angiogenic spheroids after 3 days culture of CL-MSC-*GFP-Fluc* followed by four additional days of coating with HUVEC. In hanging drops, cells coalesced into compact spheroids of 250–300 μm diameter (Supplementary Fig. S2A, B). VEGF levels of CL-MSC-*GFP-Fluc* were comparable to HUVEC when these cells were cultured in monolayer (Supplementary Fig. S2A–D). Once CL-MSC were assembled into spheroids, they expressed both VEGF monomers and dimers. This phenomenon was observed also after spheroids where coated with HUVEC for 2 and 4 days in hanging drops. We observed that VEGF monomers expression progressively reduced in spheroids and at day 7 in hanging drop culture it decreased by half of the amount seen in monolayer CL-MSC. Conversely, VEGF dimers had increased to almost double the amount seen in spheroid monomers, and remained stable throughout spheroid culture (uncoated or coated).

Angiogenic spheroids within SASG endure static 3D culture

Angiogenic spheroids were embedded in the fibrin matrix and distributed homogeneously within the graft (Supplementary Fig. S2E). SASG staining with Masson's trichrome evidenced donor cell ECM production and deposition within the spheroids (Supplementary Fig. S2F). Assessment of donor cell viability within SASG via bioluminescence imaging (BLI) after 1, 3, and 7 days in culture revealed that CL-MSC-*GFP-Fluc* in our hybrid 3D graft displayed prolonged survival in spite of thick 3D static culture. A nonsignificant decrease of CL-MSC bioluminescence was detected after 3 and 7 days of SASG culture (Supplementary Fig. S2G, H). In contrast, a significant increase of apoptotic cells was detected from day 1 (4.3% ± 3.5%) to 3 (10.7% ± 0.7%, $P < 0.05$) and from day 1 to 7 in culture (15.8% ± 6.3%, $P < 0.01$) (Supplementary Fig. S3A–D). No difference was found in the percentage of Caspase-3$^+$ cells between SASG that were 3 and 7 days in culture. Only a small amount of apoptotic cells were found within SASG after 1 day of spheroids culture within 3D grafts, which indicates that spheroids had minimal apoptosis during hanging drop culture for a week. It is possible that some of the apoptotic cells detected within spheroids embedded in SASG corresponded to HUVEC. This could explain the slight difference with our BLI results, as photon emission was exclusively captured from CL-MSC-*GFP-Fluc*. Determination of cell number (DAPI$^+$ cells) within angiogenic spheroids per section revealed that cell number within spheroids remained stable during SASG culture (Supplementary Fig. S3E). Since minimal apoptotic cells were found during the first day of SASG culture, we chose to implant SASG on the same day they were constructed in our vivo studies.

CL-MSC within SASG organized into compact cellular networks, while HUVEC displayed angiogenic sprouting in vitro

Our in vitro studies indicated that after 1 day of spheroid culture within FGs, CL-MSC adopted a MSC in vivo-like elongated shape inside the spheroids and organized into

compact cellular networks, while some HUVEC started to migrate towards the spheroid's core and to form sprouts (Supplementary Fig. S4A). At days 3 and 7 in culture HUVEC were in close contact with CL-MSC and continued progressively penetrating the spheroid's core while assembling into branches and capillary-like structures (Supplementary Fig. S4B, C). By day 7 of SASG static culture, CL-MSC started to migrate outside of the spheroid into the fibrin matrix.

Post-ischemic therapy with SASG via thoracotomy and VATS in a rat model

In total, ensued heart failure was confirmed 2 weeks after LAD ligation by echocardiography in 47 rats which were randomized for treatment. Except for untreated rats, grafts were delivered epicardially after 2 weeks of myocardial infarction either through thoracotomy: SASG and FG (Fig. 1A); or by VATS: SASG-VATS and FG-VATS (Fig. 1B–J). The overall surgical mortality rate, defined as animal death within 4 weeks of graft implantation was 11.8% (4 of 36 rats that underwent an implantation procedure, as follows: SASG, 0 of 8; FG, 2 of 10; SASG-VATS, 0 of 8; FG-VATS, 2 of 9). Mortality in untreated animals (from week 2 to 6 after LAD ligation) was 27.3% (3 of 11 MI rats). Hence, the number of rats that survived until retrieval (at 6 weeks after injury) was: MI, $n=8$; SASG, $n=8$; FG, $n=8$; SASG-VATS, $n=8$ and FG-VATS, $n=7$.

Prospective assessment of CL-MSC-*GFP-fluc* cell viability in vivo with BLI showed that donor cell survival was comparable between SASG and SASG-VATS groups (Fig. 2A–C). A nonsignificant reduction in bioluminescence was observed during the first week after graft implantation through both techniques, followed by a significant decrease in photon emission from day 1 to 14 ($8.3\times10^7\pm4.2\times10^7$ p/s vs. $5.2\times10^5\pm1.2\times10^6$ p/s, and $1.1\times10^8\pm1.0\times10^8$ p/s vs. $2.8\times10^6\pm5.8\times10^6$ p/s; $P<0.01$ and $P<0.001$). The presence of surviving CL-MSC in the LV scar area was detected 4 weeks after treatment via ex vivo BLI in explanted hearts from SASG and SASG-VATS rats (Fig. 2D).

SASG/SASG-VATS treatment preserved cardiac function and attenuated remodeling

Transthoracic echocardiography 2 weeks after induction of myocardial injury confirmed the presence of LV remodeling and deterioration of heart function in all animals, as significant increase in LV internal dimensions in systole and diastole, decrease in LV thickness and marked declines in ejection fraction (EF) and fractional shortening (FS) were found in all groups compared to baseline (Supplementary Table S1). Evaluation 4 weeks after treatment (i.e., 6 weeks after myocardial infarction) revealed that therapeutic intervention with SASG led to an enhancement of wall thickness and thickening, since values in systole and diastole increased and were comparable to baseline; whereas values in systole were significantly increased compared to week 2 in the same animals ($P<0.001$). Cardiac function was preserved in treated animals, since no further deterioration in EF and FS was observed in SASG and SASG-VATS groups from week 2 to 6 after myocardial infarction (Supplementary Table S1). A trend towards enhancement in EF from week 2 to 6 after injury was observed in SASG (14.1%) and SASG-VATS (6.2%) animals, while MI rats had a −11.4% drop in EF. FG also led to further decrease in EF by −10.53%, while FG-VATS induced a −15.77% fall in EF from week 2 to 6 after myocardial ischemia (Supplementary Table S1). Comparisons between groups at end-point revealed that SASG animals displayed thicker LV walls in systole compared to MI ($P<0.001$) and FG ($P<0.05$), while SASG-VATS animals had thicker LV walls in systole compared to MI ($P<0.05$), 4 weeks after treatment. Likewise, SASG and SASG-VATS hearts displayed significantly more conserved LV dimensions when compared to MI, both in systole and diastole, at end-point (Fig. 2E). Furthermore, FS was higher in SASG- and SASG-VATS- treated groups compared to MI ($P<0.0001$ and $P<0.01$) and to their respective FG/FG-VATS control ($P<0.01$ and $P<0.05$), 4 weeks after treatment. Similarly, EF in SASG animals (54.7%±9.6%) was higher than in MI (38.9%±6.9%, $P<0.01$), and FG (41.1%±10.3%, $P<0.05$), whereas EF in SASG-VATS animals (46.0%±6.0%) was higher than MI ($P<0.05$), 4 weeks after treatment (Fig. 2E).

SASG- and SASG-VATS-treated animals displayed significantly lower LV-end diastolic pressure compared to MI (2.56±0.8 and 3.20±0.8 mmHg vs. 5.65±1.8 mmHg; $P<0.01$ and $P<0.05$), 4 weeks after treatment (Table 1). Both SASG groups had better contractility (increased dP/dt max) compared their respective FG control groups and MI rats. Interestingly, this increase was only significant in SASG-VATS ($P<0.05$, respectively). Cardiac output (CO) in SASG (35.6±10.2 mL/min), and SASG-VATS (35.1±7.9 mL/min) animals was enhanced compared to MI rats (19.2±5.1 mL/min; $P<0.001$, respectively). SASG-treated rats also had higher CO than FG-treated rats (25.1±2.8 mL/min; $P<0.05$). Consequently, stroke volume (SV) was also significantly increased in SASG and SASG-VATS groups relative to MI ($P<0.01$ and $P<0.05$).

Effect of SASG and SASG-VATS treatment on left ventricular infarct size and vascularization

Consistent with echocardiographic evaluation, morphometric studies showed that SASG and SASG-VATS hearts had more preserved LV dimensions than the other groups (Fig. 2F). Measurement of the percentage of LV containing fibrosis revealed that treatment with SASG and SASG-VATS led to smaller LV scar size (23.23%±12.3% and 29.36%±7.93%) relative to FG and FG-VATS controls (49.36%±12.9% and 49.01%±11.7%; $P<0.01$ and $P<0.05$), and to MI hearts (56.21%±10.2%; $P<0.0001$ and $P<0.01$) (Fig. 2G).

The vascular density (number of RECA-1$^+$ blood vessels) in the LV scar area per 200× field was higher in SASG-treated hearts than FG (76.2±17.9 vs. 14.0±2.2, $P<0.001$) and MI hearts (8.0±1.9, $P<0.0001$). Similarly, SASG-VATS hearts had more vasculature (59.6±12.4) than FG-VATS (14.0±2.0, $P<0.01$), and untreated animals ($P<0.01$) (Fig. 3A–F). Also, abundant host blood vessels (RECA-1$^+$) were observed within the graft area of SASG- (Fig. 3G) and SASG-VATS-treated hearts (Fig. 3H). Likewise, a great amount of DiI$^+$ functional blood vessels with seemingly active angiogenic sprouting was observed in the graft area and LV scar area of SASG and SASG-VATS hearts (Fig. 3I–K). Quantification of blood vessel density on Masson's trichrome-stained sections showed similar results to our analysis using RECA-1

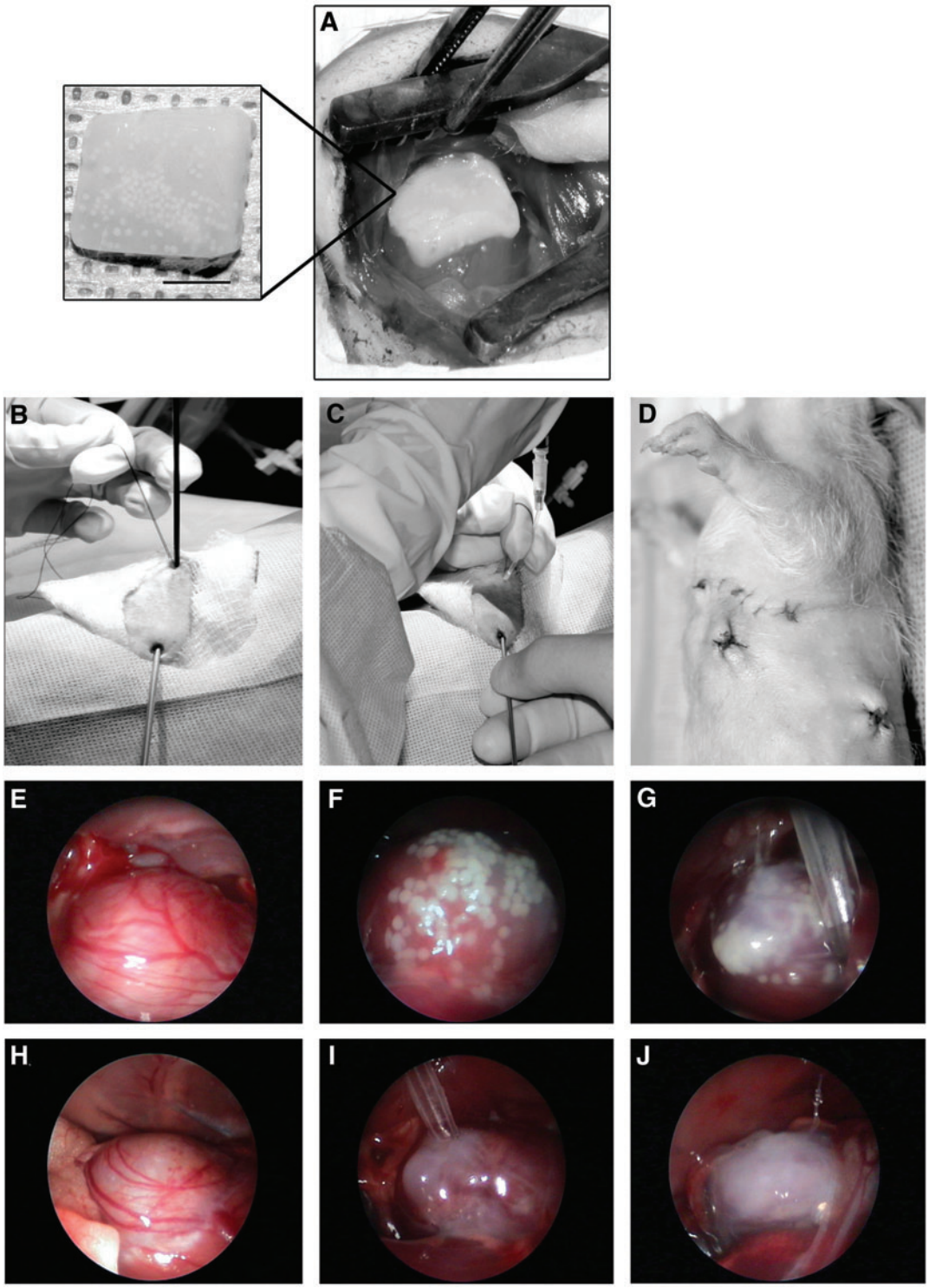

FIG. 1. Method for SASG delivery through lateral thoracotomy **(A)**, or by minimally invasive SASG-VATS **(B–G)**. **(A)** Epicardial implantation of 3D graft onto the LV scar area. *Inset* showing premade FG containing angiogenic spheroids. **(B)** For delivery of spheroids and fibrin to form an epicardial patch in situ, a 2-mm straight forward telescope was inserted through a 3-mm incision at the eighth intercostal space, mid-axillar line. **(C)** A fibrin/DPBS and spheroids mixture was loaded into a 16G catheter using a 1-mL syringe, which was then inserted into the thorax through an incision made at the fourth intercostal space, parasternal line. **(D)** Surgical wounds after VATS procedure. Note small wounds size compared to previous thoracotomy. **(E–G)** The partially gelled fibrin/DPBS/spheroids mixture was deposited epicardially onto the scar area under video-thoracoscopic visualization. The mixture was then allowed to polymerize completely before the next batch was applied. This process was repeated three times until the scar area was totally covered with spheroids. **(H–J)** The same procedure (without spheroids) was done for fibrin controls (FG-VATS). CL-MSC, cord-lining mesenchymal stem cells; SASG, subamnion-CL-MSC angiogenic spheroids-enriched grafts; FG, fibrin graft; VATS, video-assisted thoracoscopic surgery; LV, left ventricular; 3D, three-dimensional. Color images available online at www.liebertpub.com/scd

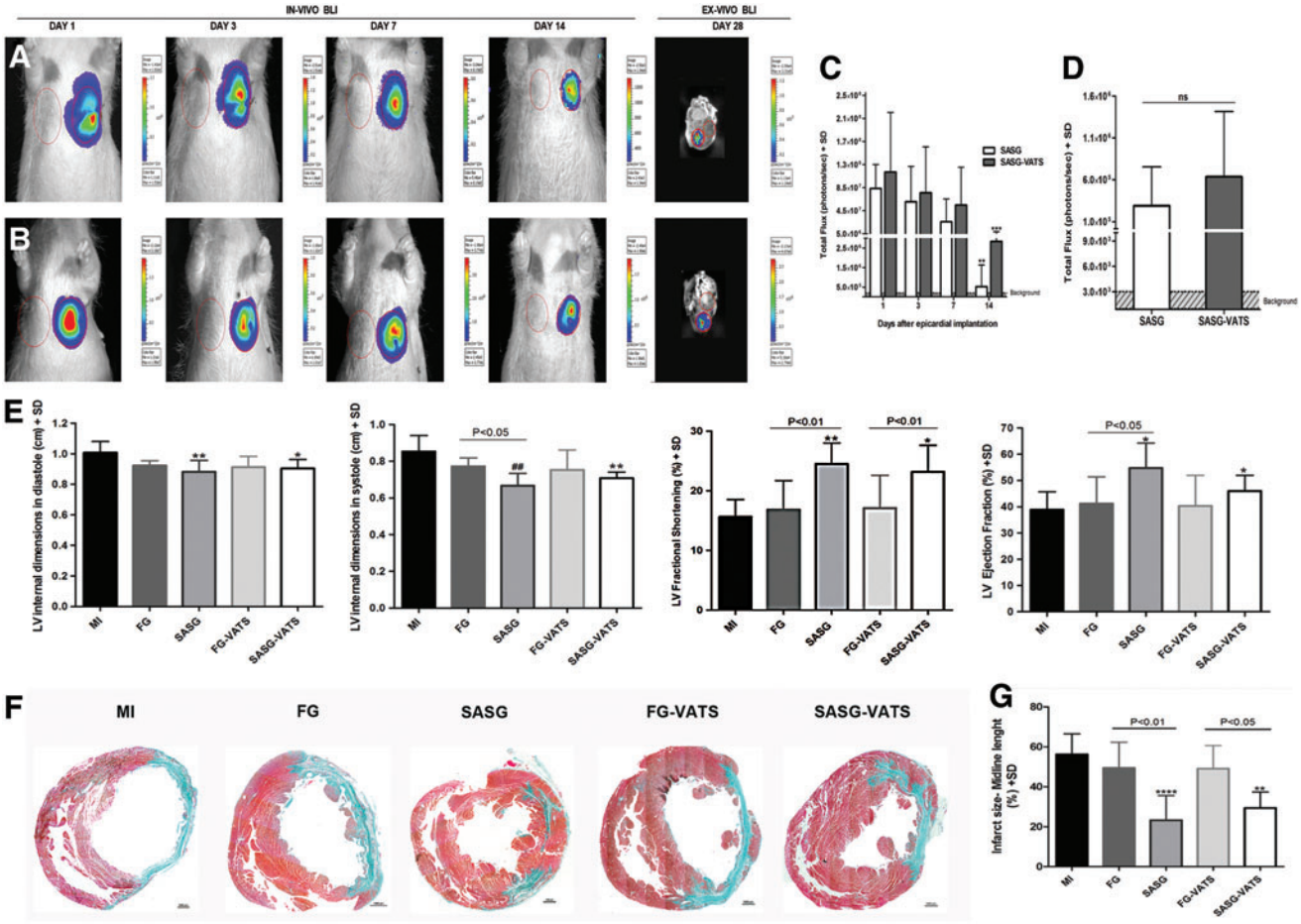

FIG. 2. In vivo and ex vivo BLI after SASG and SASG-VATS implantation. Longitudinal evaluation of donor cell viability in vivo during the first 2 weeks after **(A)** SASG and **(B)** SASG-VATS implantation. In vivo donor CL-MSC-*GFP-Fluc* viability was comparable in both SASG and SASG-VATS groups throughout the study. A nonsignificant reduction in cell viability was detected during the first week after graft implantation, followed by a significant decrease in bioluminescence from day 1 to 14 in both groups ($^{**}P < 0.01$ and $^{***}P < 0.001$) **(C)**. Ex vivo BLI 4 weeks after treatment revealed surviving donor CL-MSC in the LV scar area from both groups (*right panels* in **A, B)**, while no difference was detected in long-term donor CL-MSC survival between SASG and SASG-VATS treatment **(D)**. **(E)** Echocardiography comparison of LV remodeling and function between infarcted untreated rats (MI), FG-, SASG, FG generated in situ via VATS- (FG-VATS), and SASG-VATS-treated rats, 6 weeks after myocardial injury. SASG and SASG-VATS therapy attenuated LV adverse remodeling and preserved cardiac function 6 weeks post-injury (i.e., 4 weeks after treatment). Treated hearts displayed more conserved LV dimensions when compared to MI, both in systole and diastole, whereas significant enhancement in EF was found in SASG and SASG-VATS animals compared to MI and in SASG compared to FG. Furthermore, higher FS was observed in both treatment groups compared to MI and their respective FG controls. Significance in group comparisons versus MI is indicated as follows: $^{*}P < 0.05$; $^{**}P < 0.01$; $^{\#}P < 0.001$; $^{\#\#}P < 0.0001$. **(F)** Morphometric studies of explanted hearts 4 weeks after treatment. Representative mid-ventricular cross-section of Masson's trichrome-stained sections (40×) showing more conserved LV dimensions and LV wall thickness, as well as less scar tissue in SASG and SASG-VATS. Scale bars, 1,000 μm. **(G)** Measurement of the percentage of LV containing fibrosis (calculated by dividing the midline length of the infarcted LV wall by the midline length of total LV wall) [39] revealed that treatment with SASG and SASG-VATS led to smaller LV scar size compared to the other groups. $^{**}P < 0.01$ versus MI; $^{****}P < 0.0001$ versus MI. SD, standard deviation; GFP, green fluorescent protein; fluc, firefly luciferase; EF, ejection fraction; FS, fractional shortening; BLI, bioluminescence imaging. Color images available online at www.liebertpub.com/scd

immunostaining, as SASG and SASG-VATS treatment led to higher blood vessel density in the LV infarct area compared to all the other groups (Fig. 4A–H). This significantly higher vascularity in both groups consisted of capillaries and arterioles. SASG and SASG-VATS hearts also had increased number of arterioles at the LV border zone compared to all groups (Fig. 4I). Abundant vascularization was also observed in the engrafted epicardial patch of both SASG-treated groups (Fig. 4F–G, J–K). Consistently, a large amount of alpha-smooth muscle actin positive (α-SMA^{+}) blood vessels were observed in treated groups. These arterioles were detected throughout the LV scar area and infiltrating the grafts (Supplementary Fig. S5A–J).

In agreement with our ex vivo BLI data, engrafted CL-MSC-GFP^{+} were detected in both SASG and SASG-VATS hearts either within the ECM of the angiogenic spheroids or embedded in the FG. Donor CL-MSC were found within remnants of epicardial graft in all animals treated with

Table 1. Hemodynamic Parameters in Infarcted Untreated Rats (MI), FG-, SASG-, FG-VATS-, and SASG-VATS Treated Rats, 6 Weeks After Myocardial Injury

	MI (n = 8)	*FG* (n = 8)	*SASG* (n = 8)	*FG-VATS* (n = 7)	*SASG-VATS* (n = 8)
LVEDP (mmHg)	5.65 ± 1.75	4.17 ± 0.58	2.56 ± 0.84[b]	4.84 ± 2.98	3.20 ± 0.79[a]
Mean pressure (mmHg)	22.45 ± 3.41	23.34 ± 4.35	20.62 ± 3.75	23.70 ± 6.00	24.66 ± 4.17
Systolic duration (s)	0.10 ± 0.01	0.10 ± 0.02	0.10 ± 0.01	0.09 ± 0.01	0.09 ± 0.01
Diastolic duration (s)	0.16 ± 0.04	0.15 ± 0.04	0.17 ± 0.07	0.13 ± 0.02	0.13 ± 0.02
Cycle duration (s)	0.26 ± 0.04	0.25 ± 0.06	0.27 ± 0.07	0.22 ± 0.02	0.23 ± 0.02
Heart rate (BPM)	255.59 ± 40.23	237.89 ± 33.98	246.94 ± 44.76	272.25 ± 26.79	279.08 ± 30.56
Max dP/dt (mmHg/s)	2867.53 ± 618.84	2839.34 ± 429.85	3244.06 ± 228.33	2669.19 ± 576.28	3781.15 ± 867.58[a,e]
Min dP/dt (mmHg/s)	−2170.70 ± 415.70	−2014.07 ± 465.05	−2247.50 ± 691.02	−2006.76 ± 668.16	−2733.17 ± 776.39
Tau (ms)	19.55 ± 3.73	17.58 ± 4.91	16.46 ± 1.74	17.31 ± 2.47	16.76 ± 4.68
Cardiac output (mL/min)	19.15 ± 5.10	25.09 ± 2.79	35.56 ± 10.18[c,d]	26.30 ± 3.77	35.07 ± 7.94[c]
Stroke volume (mL/beat)	0.08 ± 0.03	0.11 ± 0.02	0.14 ± 0.04[b,d]	0.10 ± 0.01	0.13 ± 0.03[a]

Statistical significance is indicated as follows: [a]$P < 0.05$ versus MI.
[b]$P < 0.01$ versus MI.
[c]$P < 0.0001$ versus MI.
[d]$P < 0.05$ versus FG.
[e]$P < 0.05$ versus FG-VATS.
VATS, video-assisted thoracoscopic surgery; LVEDP, left ventricular end-diastolic pressure; BPM, beats per minute; FG, fibrin graft; SASG, subamnion-cord-lining mesenchymal stem cells angiogenic spheroids-enriched grafts; FG-VATS, FG generated in situ via VATS; SASG-VATS, SASG generated in situ via VATS.

SASG and SASG-VATS (Fig. 5 and Supplementary Fig. S5K–O), yet the presence of CL-MSC-GFP$^+$ in the host myocardium was only detected in five out of eight SASG-treated animals (62.5%) and in four out of eight SASG-VATS-treated rats (50%). Quantification of the number of GFP$^+$ cells in the host myocardium adjacent to the graft per animal per mm^2 was comparable between SASG (23.2 ± 11.4) and SASG-VATS (20.9 ± 8.6, $P = 0.78$) (Supplementary Fig. S5P). To note, were not able to detect donor endoglin$^+$ HUVEC within the graft or the host myocardium in any of the spheroid-treated animals.

In this study, cardiomyogenic differentiation of donor CL-MSC was not detected. Yet, some of the implanted human CL-MSC contributed to vascularization, as GFP-expressing cells were colocalized with α-SMA$^+$ cells implying smooth muscle differentiation of the CL-MSC delivered within angiogenic spheroids. These differentiated cells were observed in SASG and SASG-VATS groups, both within the scar area or the epicardial graft in proximity of the spheroid's ECM. However, CL-MSC cells that remained within the spheroids did not express α-SMA (Fig. 5). Furthermore, SASG/SASG-VATS-treated hearts had elevated percentage of PCNA$^+$ proliferating cells in the LV scar area (29.62% ± 12.6% and 18.04% ± 4.0%) relative to MI (0.24% ± 0.1%, $P < 0.05$, respectively) (Supplementary Fig. S6).

Discussion

Promising results derived from preclinical and proof-of-concept clinical trials using MSC for cardiac repair have shown their potential to alleviate the deleterious effects of myocardial ischemia [19,20], despite documented poor cell retention after cell injections [21,22]. To achieve widespread clinical application of cell-based therapies for post-ischemic heart failure, the selection of an optimal cell type combined with a therapeutically relevant timing, as well as a well optimized delivery method are crucial. Here we explore a hybrid approach that combines scaffold-free assembly of multicellular angiogenic spheroids embedded in a fibrin scaffold as a strategy to treat chronically injured myocardium. Furthermore, we compared two different mechanisms of graft delivery, and introduce a clinically relevant method for in situ assembly of epicardial grafts via minimally invasive VATS.

MSC therapy using injections or tissue engineered cardiac patches enhances LV function, attenuates adverse remodeling, and promotes angiogenesis [23–26]. We have recently shown that monodispersed CL-MSC embedded within FGs prevented further deterioration of cardiac function in failing rat hearts. Yet, the combination of CL-MSC grafts with a vascular omental flap had a synergistic effect that promoted myocardial revascularization improving thereby cardiac function and adverse remodeling [14]. In the present study, CL-MSC were used to assemble angiogenic spheroids that were then coated with HUVEC. These multicellular angiogenic spheroids exhibited increased expression of VEGF dimers, which have been recognized to have enhanced biological function and to increase endothelial cell proliferation, migration and adhesion, thereby being essential for effective angiogenesis [27,28]. Also, VEGF monomers bind to dimers under the effect of mechanical stretching forces or prehypoxic conditions leading to increased angiogenesis [29]. In our experiments, VEGF dimers normalized at day 3 of CL-MSC in hanging drops (uncoated spheroids) and remained that way at days 5 and 7 in culture upon HUVEC coating, suggesting that dimerization occurs as a direct effect of 3D gravity-enforced spheroid culture. VEGF production correlates to cell number and size of multicellular spheroids containing HUVEC as a result of hypoxia towards the core of the spheroid, apparently through a hypoxia inducible factor alpha-mediated process [11]. Three-dimensional gravity-enforced human microtissues display size-dependent VEGF expression derived from the hypoxic conditions at the spheroid's core. Hence, oversized spheroids (i.e., above 5,000

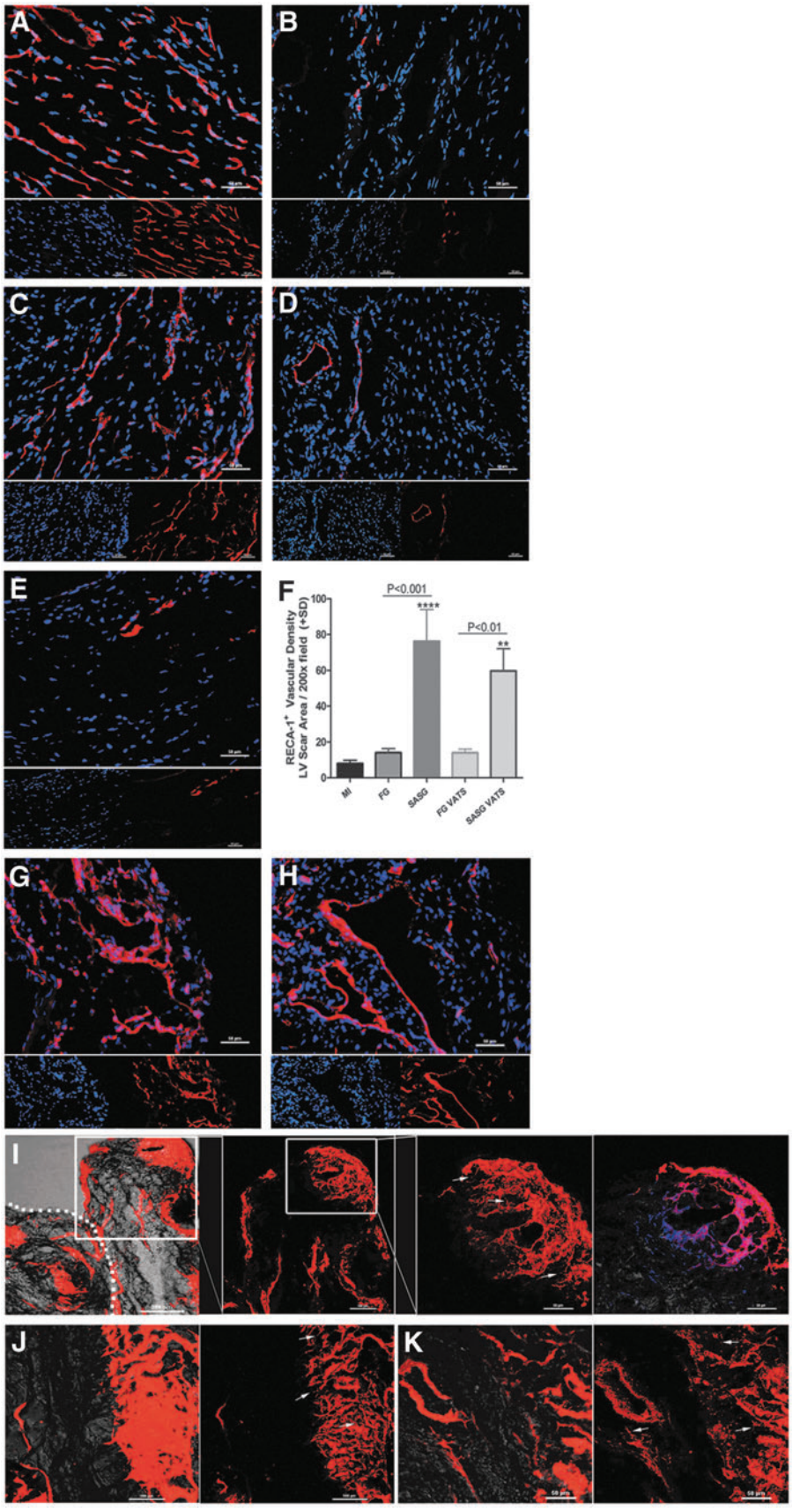

FIG. 3. Representative micrographs of the LV scar area stained with rat endothelial cell antigen-1 (RECA-1$^+$) to visualize host blood vessels in failing rat hearts treated with **(A)** SASG implanted through lateral thoracotomy; **(B)** FGs implanted by thoracotomy (FG); **(C)** SASG implanted by minimally invasive SASG-VATS; **(D)** FGs implanted though VATS (FG-VATS); or in **(E)** untreated (MI) rats, 4 weeks after treatment; (200×). RECA-1$^+$ blood vessels (*red*), nuclei (DAPI, *blue*). Scale bar indicates 50 μm. **(F)** The LV scar area in SASG and SASG-VATS contains a rich network of blood vessels. The number of RECA-1$^+$ blood vessels in the LV scar area per 200× field was higher in SASG-treated hearts than FG ($P<0.001$) and MI hearts (****$P<0.0001$). Similarly, SASG-VATS hearts had more vasculature than FG-VATS ($P<0.01$), and MI (**$P<0.01$). Host RECA-1$^+$ vasculature were also observed within the graft area of SASG **(G)** and SASG-VATS **(H)**. Confocal micrographs of the epicardial graft and LV scar area after perfusion with 1,1′-dioctadecyl-3,3,3′,3′-tetramethylindocarbocyanine perchlorate (DiI) to visualize functional blood vessels in failing rat hearts treated with SASG and SASG-VATS **(I–K)**. Merged *xy* confocal image with the transmitted light channel of the epicardial graft area showing the presence of functional blood vessels throughout the implanted graft (100×) **(I)**. *Inset* of image (200× and 400×) correspond to 3D reconstruction of *z*-stacks from the same area showing blood vessel networks surrounding and penetrating the ECM of a spheroid embedded in the graft. Abundant sprouting of neo-vessels was seen within the spheroid's ECM (*arrows*). *Dotted line* indicates host/graft interface. *Right panel* in **(I)** shows *xy* of the *inset* merged with the transmitted light channel and DAPI (*blue*). Three-dimensional images of angiogenic sprouts and pseudopodial processes at a viewing angle of 0° in the LV scar area of SASG- **(J)** and SASG-VATS-treated hearts **(K)**. *Left panel* corresponds to merged *xy* confocal image with the transmitted light channel, whereas *right panels* correspond to 3D reconstruction of *z*-stacks from the same area. *Arrows* in **(J, K)** indicate angiogenic sprouts in the LV ischemic area. ECM, extracellular matrix.

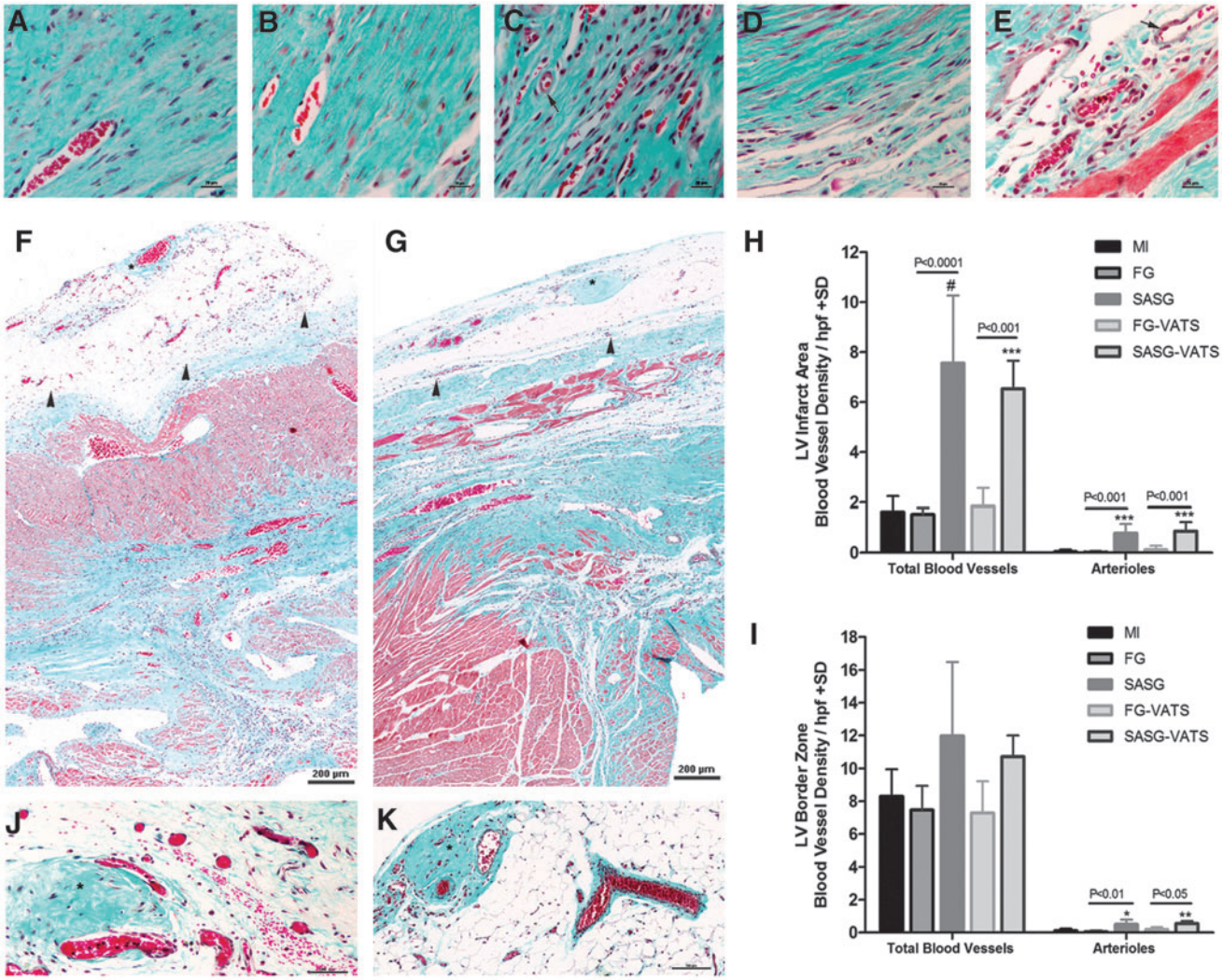

FIG. 4. Masson's trichrome-stained heart sections of **(A)** untreated MI hearts, as well as **(B)** FG-, **(C)** SASG-, **(D)** FG-VATS-, and **(E)** SASG-VATS-treated hearts 4 weeks after treatment (400×) showing more vascularity in SASG/SASG-VATS groups. *Arrows* indicate arterioles; scale bar, 20 μm. The LV wall of SASG **(F)** and SASG-VATS **(G)** had abundant blood vessels containing red blood cells (100×). *Arrowheads* indicate epicardial graft's remnants. Higher blood vessel density (arterioles and capillaries) was found in the LV infarct area (IA) of SASG/SASG-VATS hearts **(H)**. Increased arteriole counts were also found in the LV border zone (BZ) of SASG/SASG-VATS rats **(I)**. $^{*}P<0.05$ versus MI, $^{**}P<0.01$ versus MI; $^{***}P<0.001$ versus MI. $^{\#}P<0.0001$ versus MI. Rich vascularity was also observed within the graft of SASG **(F, J)** and SASG-VATS **(G, K)**, infiltrating the fibrin matrix and the spheroids' ECM (*asterisks*). Scale bar in **(J, K)**, 100 μm.

cells) tend to have self-sufficient and auto-controlled vascularization [11].

When embedded in fibrin scaffolds to generate 3D grafts, angiogenic spheroids displayed self-organization into in vivo-like tissue architecture with endothelial cell sprouting and capillary-like formation throughout the spheroid. CL-MSC within grafts had prolonged survival during the first week in vitro, as assessed by BLI. Also, cells within grafts displayed minimal apoptosis after 1 day in static 3D culture, as evidenced by active caspase-3 staining. In the current study, the rationale behind coating spheroids with HUVEC was to improve donor MSC survival. It has been shown that syngeneic rat BM-MSC microtissues (i.e., uncoated spheroids) underwent a high rate of apoptosis upon intra-myocardial injection, while microtissues made of undifferentiated MSC from mouse, rat, and human origin displayed elevated apoptosis in vitro [30]. Since incorporation of endothelial cells in multicellular spheroids prevents apoptosis [5], it is likely that HUVEC contributed to the low apoptosis rate in the angiogenic spheroids in vitro.

Intramyocardial injection of multicellular spheroids generated by other means has been recently reported in the context of myocardial repair [4,31]. Acute injection of small cell aggregates of cord blood-derived MSC (cb-MSC) improved LV function in a rodent model of myocardial infarction [4], while infarct border zone injections of small core-shell bodies made of cb-MSC and HUVEC in a thermo-responsive hydrogel system led to vasculogenesis and improvement of heart function in a rat model [31]. Contrary to these, our strategy involves oversized spheroids with high

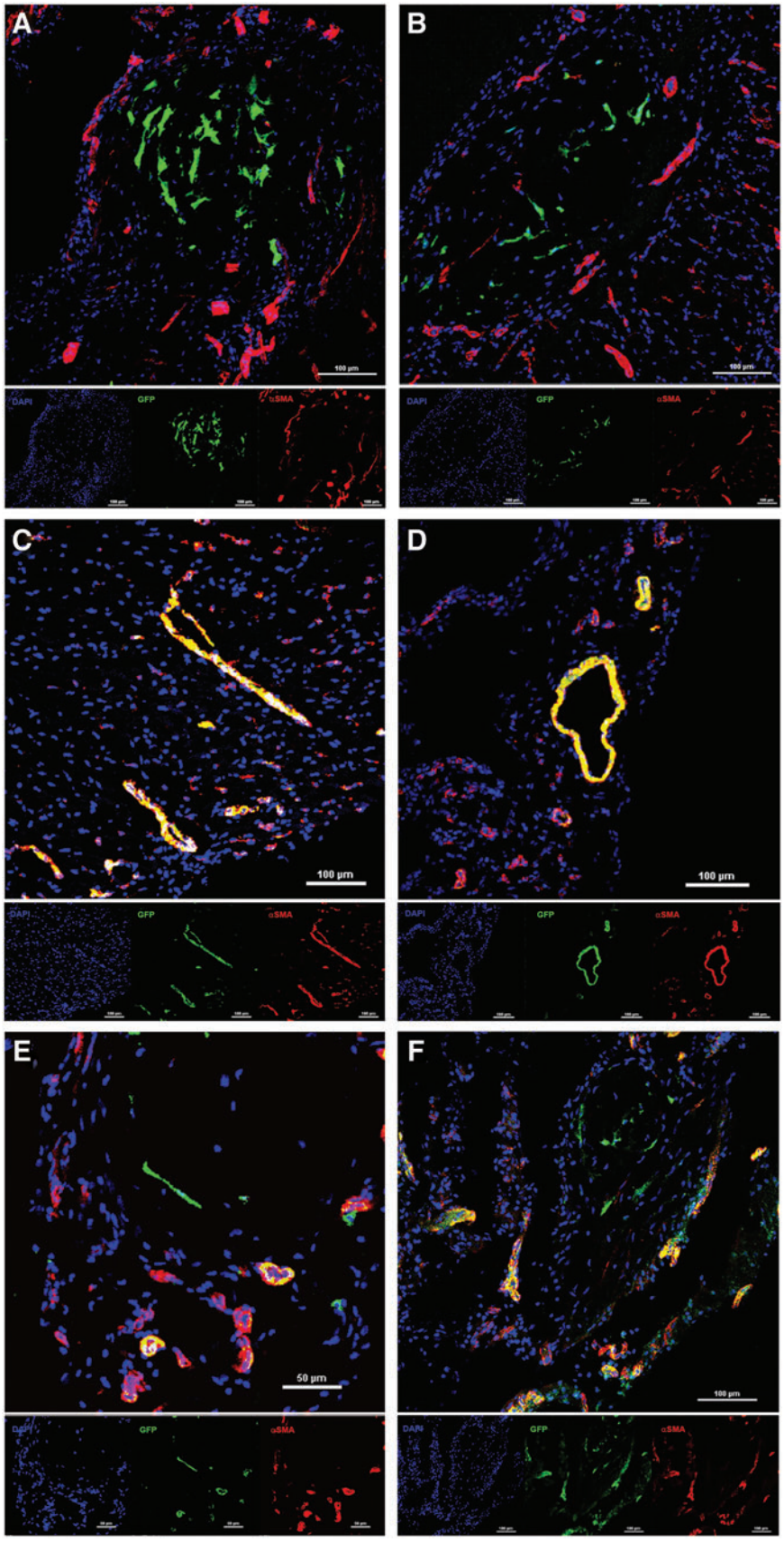

FIG. 5. Confocal micrographs of hearts that received treatment with SASG implanted through lateral thoracotomy **(A, C, E)**, or by minimally invasive SASG-VATS **(B, D, F)**, after 4 weeks of treatment showing α-SMA$^+$ blood vessels and donor CL-MSC-GFP$^+$. CL-MSC-GFP$^+$ were observed within the spheroids or within the graft in close relationship with arterioles, which tended to surround and infiltrate the spheroids **(A, B)**. Yet, some of the delivered human CL-MSC contributed to vascularization, as GFP-expressing cells were colocalized with α-SMA$^+$ cells in the LV scar **(C, D)** and graft area **(E, F)** from both groups, implying CL-MSC smooth muscle. *Top panel* shows merged image, whereas *small panel* below indicates shows each staining: α-SMA$^+$ blood vessels (*red*), CL-MSC-GFP$^+$ cells (*green*), nuclei (DAPI, *blue*). α-SMA$^+$, alpha-smooth muscle actin positive. Color images available online at www.liebertpub.com/scd

angiogenic potential embedded in a FG, which ensures stabilization of the implant and provides a substrate for engraftment while offering the possibility of minimally invasive and controlled delivery onto the LV scar area. Treatment with SASG and SASG-VATS implantation was safe, as arrhythmias were not observed during ECG evaluation immediately after treatment and at end-point, and resulted in 100% survival after 4 weeks of implantation. In vivo BLI after implantation of angiogenic subamnion-CL-MSC spheroids-enriched grafts delivered epicardially either through thoracotomy (SASG) or VATS (SASG-VATS) showed that CL-MSC donor cell survival was comparable between both groups throughout the study. An irrelevant reduction in donor cell survival was observed during the first week after graft implantation through both methods. More importantly, viable and metabolically functioning CL-MSC were detected in the LV scar area 4 weeks after treatment, confirming that our strategy favors cell retention, survival and engraftment. Furthermore, SASG and SASG-VATS prevented further remodeling and preserved cardiac function in failing rat hearts, as reflected by preserved LV dimensions and a trend towards increase in FS and EF from week 2 to 6 post-infarct. FS was significantly increased in both treatment groups compared to MI and their respective FG controls, whereas EF was higher in SASG compared to MI and FG and EF in SASG-VATS was higher relative to MI, 4 weeks after graft implantation. An enhancement in EF from week 2 to 6 after injury was observed in SASG (14.1%) and SASG-VATS (6.2%) while MI and graft control (FG/FG-VATS) groups exhibited further deterioration in EF. Although the enhancement in EF from week 2 to 6 after myocardial ischemia seen in treated groups was not significant, it might have clinical importance [1,32,33]. Improvements in EF achieved by post-ischemic cell transplantation seem to be within a similar range compared with established therapeutic strategies [32]. On the other hand, a systematic review and meta-analysis of large animal studies to evaluate the effect of post-ischemic cell therapy showed difference in EF of 7.5% at follow-up after cell therapy versus control (i.e., preservation of EF) [33]. Thus, the observed increase in EF with our current approach agrees with existing preclinical and clinical studies, and thus, its clinical relevance is clear. Improvement in LV systolic function was paralleled by decrease in LV end-diastolic pressure and enhancement in CO and SV in SASG and SASG-VATS compared to untreated rats, 4 weeks after treatment. Also, our approach led to a substantial decrease in LV scar size, and increased vascularity and arteriogenesis in the infarct area and infarct border zone compared to untreated rats and FG controls.

BM-MSC rarely display functional cardiomyogenic differentiation [34]; hence, this may not be their mechanism for cardiac regeneration. Our results demonstrate that donor CL-MSC only modestly contributed to vascularization within the ischemic hearts, or remained undifferentiated. Yet, the possibility that differentiation might have occurred by cell fusion could not be excluded. These findings differ from our previous study, as we were not able to detect CL-MSC-derived vascular differentiation in the few engrafted cells found 1 month after implantation of monodispersed CL-MSC seeded within FGs in failing rat hearts [14]. Thus, self-assembly of CL-MSC into 3D spheroids might have favored vascular differentiation. Trilineage differentiation of adult MSC after transplantation into chronically scarred myocardium has been reported [35]. Consequently, there is a common expectation that donor cells, particularly MSC, will directly participate in tissue regeneration upon implantation into the injured heart. Yet, as highlighted in the present study, improvement in vascular density in cell-treated hearts has often limited direct participation of donor cells, while a large number of transplanted cells seem to remain undifferentiated in the interstitial compartment. It has been speculated that these cells may serve as a reservoir for ongoing tissue homeostasis and play a role in maintaining blood vessel integrity [36]. We also found that SASG and SASG-VATS treatment led to cell proliferation within the LV scar area. Assembly of MSC into spheroid-like tissues exhibit E-cadherin, which regulates VEGF and mediates ERK/AKT, playing an important role in their proliferative and paracrine activity [4]. Furthermore, aggregation of human MSC into spheroids may increase their therapeutic potential by enhanced adhesion to endothelial cells and by the production of anti-inflammatory proteins [7,37,38]. Since we could not identify donor HUVEC within the FG, spheroids or host myocardium in both treatment groups, we speculate that the small amount of human endothelial cells implanted through SASG and SASG-VATS could have died even if implanted in nude rats which are to some extent permissive to the implantation of xenogeneic cells in the context of myocardial repair. Also, CL-MSC may have been more robust than HUVEC [12]. The role and fate of donor human endothelial cells in our approach would require examination of animals at early time-points after graft implantation. On the basis of our results, we speculate that besides directly contributing to vascularity, it is likely that donor CL-MSC induced angiogenesis and cell proliferation while attenuating apoptosis and collagen deposition in the ischemic myocardium. Yet, the nature of the factors responsible for the beneficial paracrine effects of the combination of CL-MSC and HUVEC spheroids applied in this study remains elusive, appealing further investigation to clarify it.

The post-acute delivery of our strategy may bear translational value, as the optimal time for cell therapy seems to be week or more after myocardial infarction with little benefit derived from early treatment [33]. Also, delivery and in situ assembly of grafts via VATS did not lead to remarkable differences in heart function and structure compared to implantation of 3D grafts through thoracotomy. Our thoracoscopic approach may hold potential for clinical application, as it might be less invasive, enables targeted cell retention and allows repeated treatment sessions. Furthermore, this method could be applicable to other strategies aiming at myocardial restoration. As the regenerative potential of allogeneic BM-MSC declines with age [28], CL-MSC may be an appealing alternative for allogeneic cell therapy in aging patients with myocardial infarction or early stage heart failure due to their high proliferative capacity in comparison to aged BM-MSC [12]. Further studies are warranted to assess the long-term effects and safety of SASG treatment for cardiac repair, while exploring the possibility of repeated treatment sessions to assure sustained long-term effects. Also, head-to-head comparisons would be necessary to determine whether the approach presented in this study is similar or superior to other tissue engineering approaches that have shown positive effects on myocardial dysfunction

(e.g., SASG vs. CL-MSC cell sheets or CL-MSC seeded in porous grafts) to explore the potential role of our findings in a wider preclinical evidence base. Also, MSC of different origin (e.g., Wharton's jelly-, cb-, BM- and adipose tissue-derived MSC) should be used to construct spheroids and test our proposed hybrid tissue engineering approach. Likewise, a large animal model exploring the in situ tissue engineering strategy presented in this study is warranted to prove its translational potential.

In conclusion, SASG treatment leads to myocardial revascularization, contributing to greater viable myocardium and less scar tissue while ameliorating heart dysfunction. We demonstrate for the first time that graft implantation via VATS is nearly as effective as epicardial delivery trough thoracotomy.

Acknowledgments

Microscopy data and imaging for this study using a Nikon A1R confocal microscope were acquired and processed in the SBIC-Nikon Imaging Centre at Biopolis, Singapore. The authors would like to thank Ms. Mary Joyce Galupo and Ms. Geronica Songco (Cardiac Department, National University Heart Centre, Singapore) for their technical support. This research was supported by the Singapore Ministry of Health's National Medical Research Council (NMRC) under its New Investigator Grant (NIG) awarded to Dr. Eliana C. Martinez (NMRC/NIG/0040/2008). The abstract for this study was presented at the American Heart Association Scientific Sessions, Nov 2012. Circulation 2012;126:A14112.

Author Disclosure Statement

T.T.P. is the founder and shareholder of CellResearch Corp Pte, Ltd.

E.C.M., T.D.V., S.L., L.H.L., S.U.G., A.L.T., C.N.L., T.K.: no competing financial interests exist.

References

1. Strauer BE and G Steinhoff. (2011). 10 Years of intracoronary and intramyocardial bone marrow stem cell therapy of the heart: from the methodological origin to clinical practice. J Am Coll Cardiol 58:1095–1104.
2. Iso Y, JL Spees, C Serrano, B Bakondi, R Pochampally, YH Song, BE Sobel, P Delafontaine and DJ Prockop. (2007). Multipotent human stromal cells improve cardiac function after myocardial infarction in mice without long-term engraftment. Biochem Biophys Res Commun 354: 700–706.
3. Bartosh TJ, Z Wang, AA Rosales, SD Dimitrijevich and RS Roque. (2008). 3D-model of adult cardiac stem cells promotes cardiac differentiation and resistance to oxidative stress. J Cell Biochem 105:612–623.
4. Lee EJ, SJ Park, SK Kang, GH Kim, HJ Kang, SW Lee, HB Jeon and HS Kim. (2012). Spherical bullet formation via E-cadherin promotes therapeutic potency of mesenchymal stem cells derived from human umbilical cord blood for myocardial infarction. Mol Ther 20:1424–1433.
5. Korff T and HG Augustin. (1998). Integration of endothelial cells in multicellular spheroids prevents apoptosis and induces differentiation. J Cell Biol 143:1341–1352.
6. Banfi A, A Muraglia, B Dozin, M Mastrogiacomo, R Cancedda and R Quarto. (2000). Proliferation kinetics and differentiation potential of ex vivo expanded human bone marrow stromal cells: Implications for their use in cell therapy. Exp Hematol 28:707–715.
7. Frith JE, B Thomson and PG Genever. (2010). Dynamic three-dimensional culture methods enhance mesenchymal stem cell properties and increase therapeutic potential. Tissue Eng Part C Methods 16:735–749.
8. Scadden DT. (2006). The stem-cell niche as an entity of action. Nature 441:1075–1079.
9. Anderer U and J Libera. (2002). In vitro engineering of human autogenous cartilage. J Bone Miner Res 17:1420–1429.
10. Kelm JM, V Djonov, SP Hoerstrup, CI Guenter, LM Ittner, F Greve, A Hierlemann, CD Sanchez-Bustamante, JC Perriard, E Ehler and M Fussenegger. (2006). Tissue-transplant fusion and vascularization of myocardial microtissues and macrotissues implanted into chicken embryos and rats. Tissue Eng 12:2541–2553.
11. Kelm JM, C Diaz Sanchez-Bustamante, E Ehler, SP Hoerstrup, V Djonov, L Ittner and M Fussenegger. (2005). VEGF profiling and angiogenesis in human microtissues. J Biotechnol 118:213–229.
12. Deuse T, M Stubbendorff, K Tang-Quan, N Phillips, MA Kay, T Eiermann, TT Phan, HD Volk, H Reichenspurner, RC Robbins and S Schrepfer. (2011). Immunogenicity and immunomodulatory properties of umbilical cord lining mesenchymal stem cells. Cell Transplant 20:655–667.
13. Bueno H, JS Ross, Y Wang, et al. (2010). Trends in length of stay and short-term outcomes among medicare patients hospitalized for heart failure, 1993–2006. JAMA 303:2141–2147.
14. Lilyanna S, EC Martinez, TD Vu, LH Ling, SU Gan, AL Tan, TT Phan and T Kofidis. (2013). Cord lining-mesenchymal stem cells graft supplemented with an omental flap induces myocardial revascularization and ameliorates cardiac dysfunction in a rat model of chronic ischemic heart failure. Tissue Eng Part A 19:1303–1315.
15. Martinez EC, J Wang, S Lilyanna, LH Ling, SU Gan, R Singh, CN Lee and T Kofidis. (2013). Post-ischaemic angiogenic therapy using in vivo prevascularized ascorbic acid-enriched myocardial artificial grafts improves heart function in a rat model. J Tissue Eng Regen Med 7:203–212.
16. Dominici M, K Le Blanc, I Mueller, I Slaper-Cortenbach, F Marini, D Krause, R Deans, A Keating, D Prockop and E Horwitz. (2006). Minimal criteria for defining multipotent mesenchymal stromal cells. The International Society for Cellular Therapy position statement. Cytotherapy 8:315–317.
17. Kofidis T, JL de Bruin, G Hoyt, DR Lebl, M Tanaka, T Yamane, CP Chang and RC Robbins. (2004). Injectable bioartificial myocardial tissue for large-scale intramural cell transfer and functional recovery of injured heart muscle. J Thorac Cardiovasc Surg 128:571–578.
18. Vu DT, LK Ti, LC Ong, PH Neo, CN Lee and T Kofidis. (2012). Novel sutureless mitral valve implantation method involving a bayonet insertion and release mechanism: a proof of concept study in pigs. J Thorac Cardiovasc Surg 143:985–988.
19. Schuleri KH, GS Feigenbaum, M Centola, ES Weiss, JM Zimmet, J Turney, J Kellner, MM Zviman, KE Hatzistergos, et al. (2009). Autologous mesenchymal stem cells produce reverse remodelling in chronic ischaemic cardiomyopathy. Eur Heart J 30:2722–2732.
20. Williams AR, B Trachtenberg, DL Velazquez, I McNiece, P Altman, D Rouy, AM Mendizabal, PM Pattany, GA Lopera, et al. (2011). Intramyocardial stem cell injection in patients with ischemic cardiomyopathy: functional recovery and reverse remodeling. Circ Res 108:792–796.

21. Wang W, Q Jiang, H Zhang, P Jin, X Yuan, Y Wei and S Hu. (2011). Intravenous administration of bone marrow mesenchymal stromal cells is safe for the lung in a chronic myocardial infarction model. Regen Med 6:179–190.
22. Li SH, TY Lai, Z Sun, M Han, E Moriyama, B Wilson, S Fazel, RD Weisel, T Yau, JC Wu and RK Li. (2009). Tracking cardiac engraftment and distribution of implanted bone marrow cells: comparing intra-aortic, intravenous, and intramyocardial delivery. J Thorac Cardiovasc Surg 137:1225–1233.e1.
23. Tomita S, DA Mickle, RD Weisel, ZQ Jia, LC Tumiati, Y Allidina, P Liu and RK Li. (2002). Improved heart function with myogenesis and angiogenesis after autologous porcine bone marrow stromal cell transplantation. J Thorac Cardiovasc Surg 123:1132–1140.
24. Kinnaird T, E Stabile, MS Burnett, CW Lee, S Barr, S Fuchs and SE Epstein. (2004). Marrow-derived stromal cells express genes encoding a broad spectrum of arteriogenic cytokines and promote in vitro and in vivo arteriogenesis through paracrine mechanisms. Circ Res 94:678–685.
25. Reffelmann T, M Dorr, H Volzke, J Kors, J Ruppert, D Robinson and SB Felix. (2009). Combination of electrocardiographic and echocardiographic information identifies individuals prone to a progressive increase in left ventricular mass over 5 years. J Hypertens 27:861–868.
26. Huang NF, A Lam, Q Fang, RE Sievers, S Li and RJ Lee. (2009). Bone marrow-derived mesenchymal stem cells in fibrin augment angiogenesis in the chronically infarcted myocardium. Regen Med 4:527–538.
27. Khan M, S Akhtar, S Mohsin, N Khan S and S Riazuddin. (2011). Growth factor preconditioning increases the function of diabetes-impaired mesenchymal stem cells. Stem Cells Dev 20:67–75.
28. Khan M, S Mohsin, SN Khan and S Riazuddin. (2011). Repair of senescent myocardium by mesenchymal stem cells is dependent on the age of donor mice. J Cell Mol Med 15: 1515–1527.
29. Hare JM, JE Fishman, G Gerstenblith, DL DiFede Velazquez, JP Zambrano, VY Suncion, M Tracy, E Ghersin, PV Johnston, et al. (2012). Comparison of allogeneic vs autologous bone marrow-derived mesenchymal stem cells delivered by transendocardial injection in patients with ischemic cardiomyopathy: the POSEIDON randomized trial. JAMA 308: 2369–2379.
30. Kelm JM, M Breitbach, G Fischer, B Odermatt, I Agarkova, BK Fleischmann and SP Hoerstrup. (2012). 3D microtissue formation of undifferentiated bone marrow mesenchymal stem cells leads to elevated apoptosis. Tissue Eng Part A 18: 692–702.
31. Lee WY, HJ Wei, JJ Wang, KJ Lin, WW Lin, DY Chen, CC Huang, TY Lee, HY Ma, et al. (2012). Vascularization and restoration of heart function in rat myocardial infarction using transplantation of human cbMSC/HUVEC core-shell bodies. Biomaterials 33:2127–2136.
32. Reffelmann T, S Konemann and RA Kloner. (2009). Promise of blood- and bone marrow-derived stem cell transplantation for functional cardiac repair: putting it in perspective with existing therapy. J Am Coll Cardiol 53:305–308.
33. van der Spoel TI, SJ Jansen of Lorkeers, P Agostoni, E van Belle, M Gyongyosi, JP Sluijter, MJ Cramer, PA Doevendans and SA Chamuleau. (2011). Human relevance of pre-clinical studies in stem cell therapy: systematic review and meta-analysis of large animal models of ischaemic heart disease. Cardiovasc Res 91:649–658.
34. Siegel G, P Krause, S Wohrle, P Nowak, M Ayturan, T Kluba, BR Brehm, B Neumeister, D Kohler, et al. (2012). Bone marrow-derived human mesenchymal stem cells express cardiomyogenic proteins but do not exhibit functional cardiomyogenic differentiation potential. Stem Cells Dev 21:2457–2470.
35. Quevedo HC, KE Hatzistergos, BN Oskouei, GS Feigenbaum, JE Rodriguez, D Valdes, PM Pattany, JP Zambrano, Q Hu, et al. (2009). Allogeneic mesenchymal stem cells restore cardiac function in chronic ischemic cardiomyopathy via trilineage differentiating capacity. Proc Natl Acad Sci USA 106:14022–14027.
36. da Silva Meirelles L, AI Caplan and NB Nardi. (2008). In search of the in vivo identity of mesenchymal stem cells. Stem Cells 26:2287–2299.
37. Potapova IA, PR Brink, IS Cohen and SV Doronin. (2008). Culturing of human mesenchymal stem cells as three-dimensional aggregates induces functional expression of CXCR4 that regulates adhesion to endothelial cells. J Biol Chem 283:13100–13107.
38. Bartosh TJ, JH Ylostalo, A Mohammadipoor, N Bazhanov, K Coble, K Claypool, RH Lee, H Choi and DJ Prockop. (2010). Aggregation of human mesenchymal stromal cells (MSCs) into 3D spheroids enhances their antiinflammatory properties. Proc Natl Acad Sci USA 107:13724–13729.
39. Takagawa J, Y Zhang, ML Wong, RE Sievers, NK Kapasi, Y Wang, Y Yeghiazarians, RJ Lee, W Grossman and ML Springer. (2007). Myocardial infarct size measurement in the mouse chronic infarction model: comparison of area- and length-based approaches. J Appl Physiol 102:2104–2111.

Address correspondence to:
Dr. Eliana C. Martinez
Department of Surgery
Yong Loo Lin School of Medicine
National University of Singapore
1E Kent Ridge Road
NUHS Tower Block, Level 8
Singapore 119228
Singapore

E-mail: eliana_martinez@nuhs.edu.sg

Received for publication March 5, 2013
Accepted after revision July 19, 2013
Prepublished on Liebert Instant Online July 19, 2013